 doi:10.20944/preprints202210.0436.v1

Article

Assessment Of 3D Printed Polycaprolactone, Hydroxyapatite Nanoparticles and Polyethylene Glycol Diacrylate Scaffolds for Bone Regeneration

Ana Catarina Sousa [1,2,3], Sara Biscaia [4], Rui Alvites [1,2,3], Mariana Branquinho [1,2,3], Bruna Lopes [1,2,3], Patrícia Sousa [1,2,3], Joana Valente [4], Margarida Franco [4], José Domingos Santos [5,6], Carla Mendonça[1,2,3], Luís Atayde [1,2,3], Nuno Alves [4,†] and Ana Colette Maurício [1,2,3,†,*]

[1] Veterinary Clinics Department, Abel Salazar Biomedical Sciences Institute (ICBAS), Porto, Portugal; ana-catarinasoaressousa@hotmail.com (A.C.S.); ruialvites@hotmail.com (R.A.); m.esteves.vieira@gmail.com (M.B.); brunisabel95@gmail.com (B.L); pfrfs_10@hotmail.com (P.S.)
[2] Animal Science Studies Centre (CECA), Agroenvironment, Technologies and Sciences Institute (ICETA), University of Porto (UP), Rua D. Manuel II, Apartado 55142, 4051-401 Porto, Portugal
[3] Associate Laboratory for Animal and Veterinary Sciences (AL4AnimalS), Lisbon, Portugal
[4] Centre for Rapid and Sustainable Product Development (CDRSP), Polytechnic of Leiria, 2411-901 Leiria, Portugal; sara.biscaia@ipleiria.pt (S.B.); joana.valente@ipleiria.pt (J.F.A.V.); margarida.franco@ipleiria.pt (M.F.); nuno.alves@ipleiria.pt (N.A.)
[5] REQUIMTE-LAQV, Departamento de Engenharia Metalúrgica e Materiais, Faculdade de Engenharia, Universidade do Porto, Rua Dr. Roberto Frias, 4200-465, Porto, Portugal; jdsantos@fe.up.pt (J.D.S.)
† These authors contributed equally to this work.
* Correspondence: ana.colette@hotmail.com/acmauricio@icbas.up.pt (A.C.M)

Abstract: Notwithstanding the advances achieved in the last decades in the field of synthetic bone substitutes, the development of biodegradable 3D scaffolds with ideal mechanical and biological properties remains an unattained challenge. In this work, a novel approach is explored to produce synthetic bone grafts mimicking the complex bone structure using additive manufacturing. For the first time, scaffolds were produced, using an extrusion technique, composed of a thermoplastic polymer, polycaprolactone (PCL), hydroxyapatite nanoparticles (HANp), and polyethylene glycol diacrylate (PEGDA). These scaffolds were further compared with two groups of scaffolds: one composed of PCL and another of PCL and HANp. After production, optimisation and characterisation of these scaffolds, an *in vitro* evaluation was performed using human dental pulp stem/stromal cells (hDPSCs). Through the findings it was possible to conclude that PEGDA scaffolds were successfully produced presenting networks of interconnected channels, presenting hydrophilic properties (15.15 ± 4.06°), adequate mechanical performance (10.41MPa ± 0.934), and allowing a cell viability significantly superior to the other groups analysed. To conclude, findings in this study demonstrated that PCL, HANp and PEGDA scaffolds may have promising effects on bone regeneration and might open new insights for 3D tissue substitutes.

Keywords: Additive manufacturing; Biomaterials; Bone; Bone regeneration; Critical Bone Defects; Hydroxyapatite nanoparticles; Polycaprolactone; Polyethylene glycol diacrylate; Scaffolds

1. Introduction

The population aging leads to a remarkable increase in the number of degenerative diseases, osteogenic disorders, fractures, and bone infections [1,2]. Although bone tissue can heal itself to a certain extent following bone pathology, when it concerns critical-sized defects (above about 3 cm), it may not be fully restored [3-5]. Particularly in such cases, the reconstruction of bone defects, with mechanical integrity to the original surrounding bone tissues is essential for a patient's rehabilitation [6]. Therefore, the search for new solutions has focused on tissue engineering through the development of three-dimensional

 doi:10.20944/preprints202210.0436.v1

(3D) structures, namely scaffolds for the regeneration of bone tissues [7-10]. Some properties must be considered when producing scaffolds for bone regeneration: (a) biocompatibility devoid of unchained negative biological response in the body; (b) osteoconduction to promote cell adhesion and bone growth; (c) biodegradability to ensure controlled replacement of the biomaterial by the neoformed bone; (d) mechanical properties to ensure support during bone bridging; (e) sterility of the material ; and (f) appropriate design in terms of porosity, interconnectivity and pore size to provide the cell proliferation and angiogenesis [11-15]. In addition to the development of biomaterial support, cells and growth factors have an important role in the formation of biological substitute, so it is necessary to resort to regenerative medicine and tissue engineering [16]. The use of biomaterials with mesenchymal stem cells (MSCs) allows the proliferative and differentiation capacities of the latter to work in synergy with scaffolding properties [1,17].

According to the literature, synthetic rigid porous scaffolds have usually been made based on hydroxyapatite nanoparticles (HANp), biphasic calcium phosphate (BCP), beta-tricalcium phosphate (β-TCP), and polycaprolactone (PCL) [18-21]. Several studies combined PCL and HANp in scaffolds due to their properties and achieved good results inherent to bone regeneration both *in vitro* and *in vivo* [22-31]. PCL has been widely used due to its good biocompatibility, biodegradability, ease of processing (melting point between 55 and 60°C) and the fact that its blends well with other materials such as ceramics [32-34]. Furthermore, HANp, as a biomaterial, presents good stability, biocompatibility, degradability, promotes adhesion/proliferation of osteoblasts and has the potential to form chemical bonds with the bone itself [35-38]. Previous studies, consider PEGDA hydrogel as an effective biomaterial in bone regeneration due to its properties such as strength, gelation process, hydrophilicity, and cell adhesion [39-44].

Today, several additive manufacturing techniques are used to produce complex bone implants, namely, selective laser sintering, selective laser melting, stereolithography, electron beam melting, electrospinning, and fused deposition modelling [45]. Fused deposition modelling, commonly known as extrusion-based processes, is a promising 3D printing and manufacturing technique in the production of interconnected porous scaffolds [46]. This technique is easy to operate, safe, reliable, has controllable, and the produced structures normally have good mechanical properties [4].

For the present study, combined scaffolds of PCL, HANp, and PEGDA were produced by an extrusion additive manufacturing system. Subsequently, the surface chemistry of 3D printed scaffolds was characterised using Fourier Transform Infrared Spectroscopy (FTIR) and Contact Angle Measurement. The morphological properties were evaluated by X-ray Micro-computed Tomography (Micro-CT), Scanning Electron Microscopy (SEM) and Energy Dispersive X-ray Spectroscopy (EDX). Moreover, compression tests were performed to assess the mechanical response of the scaffolds. Scaffolds were further characterised *in vitro*, assessing their cytocompatibility properties. This study lays the groundwork for future research into the use of these three materials for more accelerated and effective bone regeneration.

2. Materials and Methods

2.1. Materials

PCL (CAPA® 6500) from Perstorp Caprolactones (Cheshire, United Kingdom) (Mw: 50 kDa) and HANp (particle size < 200 nm) from Sigma-Aldrich (Saint Louis, USA), were used. Formulations were produced using N,N-Dimethylformamide (DMF) from CHEM-LAB (Belgium) and by the solvent casting technique. For the hydrogel formulation, PEGDA, from Sigma-Aldrich (Saint Louis, USA), Mn= 750 (mol) and HEPES solution (Gibco, 15140122) were used. Photopolymerization was induced using 0.1% w/V 2-Hydroxy-4′-(2-hydroxyethoxy)-2-methylpropiophenone 98% (Irgacure 2959, Sigma-Aldrich) photoinitiator at UV light (365 nm) exposure.

Preprints (www.preprints.org) | NOT PEER-REVIEWED | Posted: 28 October 2022 doi:10.20944/preprints202210.0436.v1

2.2. Sample Design

To develop the scaffolds, protocols were designed, relying on available literature revised [47-50]. In the present work, a biomanufacturing system (Biomate Project from ANI), developed by the CDRSP-IPLeiria, was used [47,50-58]. This equipment integrates three biomanufacturing techniques: micro-extrusion system, multi-head dispensing system and electrospinning [48] . Three different matrices were produced in this system: i) PCL scaffolds; ii) PCL scaffolds with the addition of HANp; and iii) PCL/HANp scaffolds submerged in PEGDA solution.

For the production of the scaffolds, a nozzle with a diameter of 400 μm was used. The parameters employed were 240 mm/s of deposition velocity, 9 rpm of screw rotation velocity and 85°C of liquefier temperature. The methodologies used in the production of the scaffolds (diameter: 10 mm, height: 3 mm, and pore size: 380 μm) were as follows:

i) PCL scaffolds;

The PCL was dissolved in DMF at 80°C and dried in a controlled environment for 96 hours. The membranes were cut into pieces to be subsequently placed in the bioextrusion equipment deposit.

ii) PCL scaffolds with the addition of hydroxyapatite nanoparticles (HANp);

PCL (60 wt%) and HANp (40 wt%) were dissolved in DMF and dried in a controlled environment. The completely dried membranes were cut into pieces to be subsequently placed in the bioextrusion equipment deposit.

iii) PCL/HANp scaffolds submerged in PEGDA solution.

For PCL/HANp scaffolds, the same procedure previously mentioned in point ii, was employed. The PEGDA (6 wv% in deionized water), Hepes and Irgacure 2959 solution was made by melt blending at 50°C, using a heating plate with stirrer. Afterwards, the PCL/HANp scaffolds were submerged in the previously made solution. The scaffolds were carefully removed from the solution and were crosslinked using UV light exposure (365 nm). The schematic representation of the procedure is summarized in Figure 1.

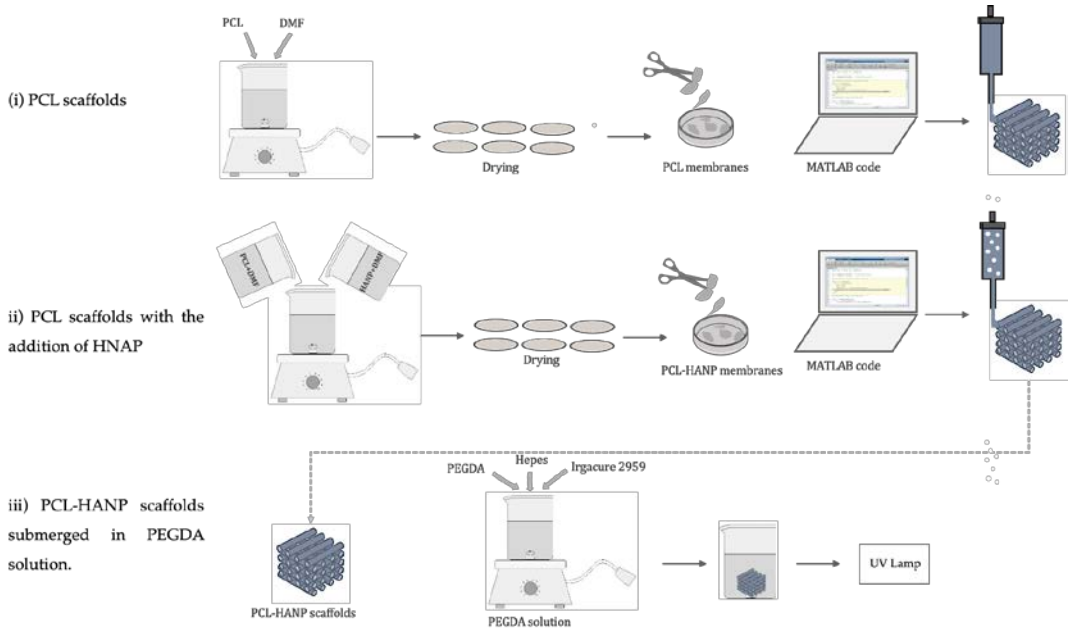

Figure 1. Schematic representation of the process for the manufacture of scaffolds.

 doi:10.20944/preprints202210.0436.v1

2.3. Material Characterisation

The physical, chemical, and mechanical characterisation of the produced scaffolds was performed: Fourier-Tranform Infrared Spectroscopy (FTIR), contact angle measurement, Micro-Computed Tomography (Micro-CT), Scanning Electron Microscopy (SEM), Energy Dispersive X-ray analysis (EDX), and compression tests.

2.3.1. Fourier-transform infrared spectroscopy

To extract qualitative chemical information, samples were analysed using the Bruker Alpha-P ATR FTIR spectrometer. The tests were carried out at room temperature, in a spectral range of 400–4000 cm^{-1}, with a resolution of 4 cm^{-1} in a total of 64 scans.

2.3.2. Contact Angle Measurement

The wettability of the formulations was evaluated by static contact angle measurement at 10s on a Theta Lite optical tensiometer (Attension, Finland). A water droplet was dispensed on the surface of solid samples and the contact angle was measured by OneAttension 2.1 software (Attension).

2.3.3. X-ray micro-computed Tomography

Micro-CT scans of the scaffolds were performed using a SkyScan microtomograph model 1174 by Brucker Company (Brussels, Belgium). The scaffolds were scanned using the following parameters:

i. For PCL (formulation and scaffolds scans): 50 Kv; 800 μA; 19.6 image pixel size; 4500 ms; averaging frames 3; 0.9 rotation degree; no filter;
ii. For PCL/HANp and PCL/HANp scaffolds submerged in PEGDA solution (formulation and scaffolds scans): 50 Kv; 800 μA; 19.6 image pixel size; 6500 ms; averaging frames 3; 0.9 rotation degree; 0.25; Al filter.

Reconstructions, 3D images and porosity assessment were carried out through NRecon (v 1.7.0.4), CTVox (v 3.2.0) and CTAn (v 1.20) softwares, respectively.

2.3.4. Scanning Electron Microscopy and Energy Dispersive X-ray analysis

To analyze the filament and pore morphology, scaffolds from each experimental group were analysed by SEM using a Vega3 Tescan equipment (Tescan, Brno, Czechia), operating at an accelerating voltage of 20 kV, at variable magnifications. The samples were fixed on a brass stub using double-sided tape and then made electrically conductive by coating with gold/palladium (Au/Pd) thin film, by sputtering, using the sputter coater equipment (Quorum Technologies). The samples were also analysed using EDX (Xflash 6|30 from Brucker).

2.3.5. Mechanical Analysis

Compression tests were performed to evaluate the mechanical properties of each scaffold. The tests were conducted according to ASTM STP 1173 standards, using a TA.XTplusC, with using an extension rate of 0.6 mm/min. Mechanical testing was carried out using six scaffolds samples, with a diameter of 10 mm and a height of 3 mm. Stress (MPa) data was computed from load-displacement measurements.

2.4. In Vitro Tests

2.4.1. Cell culture and maintenance

The human dental pulp stem/stromal cells (hDPSCs) used in this study were sourced from AllCells, LLC (Cat. DP0037F, Lot No. DPSC090411-01). These were maintained in MEM α, GlutaMAX™ Supplement, nucleoside-free (Gibco, 32561029). This medium was supplemented with 10% (v/v) fetal bovine serum (FBS) (Gibco, A3160802), 100 IU/ml penicillin, 0.1 mg/ml streptomycin (Gibco, 15140122), 2.05 μm/ml amphotericin B (Gibco,

Preprints (www.preprints.org) | NOT PEER-REVIEWED | Posted: 28 October 2022 doi:10.20944/preprints202210.0436.v1

15290026) and 10 mM HEPES buffer solution (Gibco, 15630122). DPSCs were maintained in standard conditions, namely at 37°C, 80% humidified atmosphere and 5% CO_2.

2.4.2. Cytocompatibility assessment

Prior to cytocompatibility tests, all scaffolds in this study were sterilised by gamma radiation (25 kGy) in a Red Perspex Dosimeter. Then, the samples were tested with hDPSCs using the PrestoBlue™ viability to assess the impact of the scaffolds on cell adhesion and viability. This reagent is a commercially available, ready-to-use, water-soluble, resazurin-based solution (7-hydroxy-3H-phenoxazin-3-one-10-oxide). The active cells reduce this compound into resazurin, a process that is accompanied by a change in the colour and fluorescence of the solution. Consequently, absorbance measurements of the solution indicate viability, thus allowing quantitative measurement of cell proliferation. Due to the reduction of the compound by the viable cells, the solution colour changes from blue to a reddish tone. Thus, changes in cell viability/proliferation were assessed by corresponding changes in absorbance measurements [59].

In brief, scaffolds were seeded using dynamic seeding, i.e., these were incubated in cell suspension (density of $2.5x10^5$ per scaffold) on a roller bench all overnight at 37°C, 80% humidified atmosphere and 5% CO_2 environment. Later, the seeded scaffolds were moved to a 24-well non-adherent plate and submerged in fresh complete medium. Presto Blue™ evaluation was performed at different time-points: 24, 72, 120 and 168 hours. Thus, for each time point, culture media was removed from each well and replaced with fresh complete medium with 10% (v/v) of the PrestoBlue™ reagent (Invitrogen, A13262). Cells were incubated for 1 hour at 37°C, 80% humidified atmosphere and 5% CO_2. Supernatant media were transferred to a 96-well plate and absorbance was read at 570 and 595 nm. Changes in cell viability were detected by absorbance spectroscopy in a spectrophotometer, Multiskan™ FC Microplate Photometer (Thermo Scientific™, 51119000). For each well, the absorbance at 595 nm (normalization wavelength) was subtracted from the absorbance at 570nm (experimental result). The corrected absorbance is obtained by subtracting the mean of the control wells for each experimental well. The cells were then washed in Dulbecco's phosphate buffered saline (DPBS, Sigma®, D8537) to remove any residual PrestoBlue™ and then fresh culture medium is replenished to each well. The data were analysed and subsequently normalised to the mean of the gold standard (PCL group), presented as % viability inhibition.

2.5. Statistical analysis

In this study, statistical analysis was accomplished using GraphPad Prism® (version 8.40 for Mac OS X, GraphPad Software, La Jolla California USA). Results were reported as mean ± standard error of the mean (SE). The comparisons between groups were achieved by one-way ANOVA followed by Tukey's multiple comparisons test. Differences were considered statistically significant only when $P \leq 0.05$. Significant results are denoted according to P values with one, two, three or four of the symbols (*) corresponding to $0.01 < P \leq 0.05$, $0.001 < P \leq 0.01$, $0.0001 < P \leq 0.001$ and $P \leq 0.0001$, respectively.

3. Results

3.1. Scaffolds production

In this study, three scaffolds with different composition, namely, PCL, PCL/HANp and PCL/HANp/PEGDA were manufactured by extrusion. The samples were produced by filament deposition with 10 mm diameter, 3 mm height and 380 μm pore size. Figure 2 shows 3D scaffolds representative of each group.

Preprints (www.preprints.org) | NOT PEER-REVIEWED | Posted: 28 October 2022 doi:10.20944/preprints202210.0436.v1

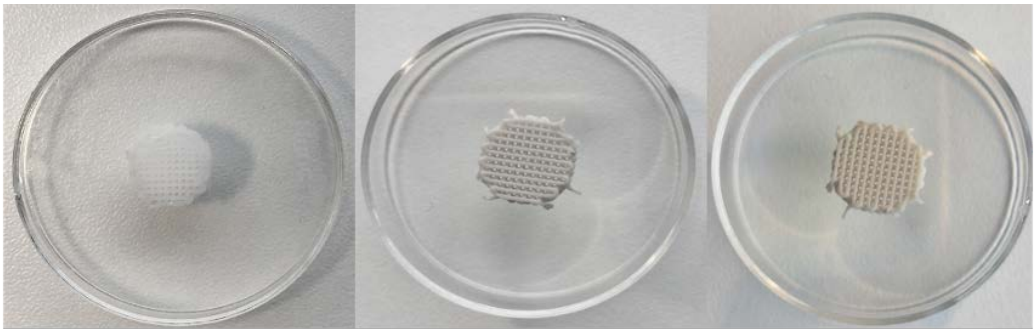

Figure 2. Observation of the 3D printed scaffolds for each group: (a) PCL scaffolds; (b) PCL scaffolds with the addition of hydroxyapatite nanoparticles; (c) PCL/HANp scaffolds submerged in PEGDA solution.

According to the results (Figure 2 a, b and c), the 3D scaffolds were successfully produced. The filaments, in all groups, seem to be well coordinated and positioned.

3.2. Material Characterisation

For the assessment of the functional groups, the samples were analysed by FTIR spectroscopy. Therefore, segments from each group (PCL, PCL/HANp, PCL/HANp/PEGDA and PEGDA) were analysed (Figure 3). In the PCL, PCL/HANp and PCL/HANp/PEGDA groups are represented the characteristic absorption bands of PCL which are asymmetric CH_2 at 2943 cm^{-1}, symmetric CH_2 at 2865 cm^{-1} and, C=O at around 1720 cm^{-1} [60,61]. Regarding HANp, in the PCL/HANp and PCL/HANp/PEGDA sample the peaks corresponding to phosphates (ν1 and ν3) around 1300 cm^{-1} and carbonates between 850 and 890 cm^{-1} are represented [60,62]. Finally, in the PCL/HANp/PEGDA sample, characteristic peaks of PEGDA are represented at 1638 cm^{-1}(double peak due to elongation of the vinyl groups), and 910 cm^{-1} and 1720 cm^{-1} [63].

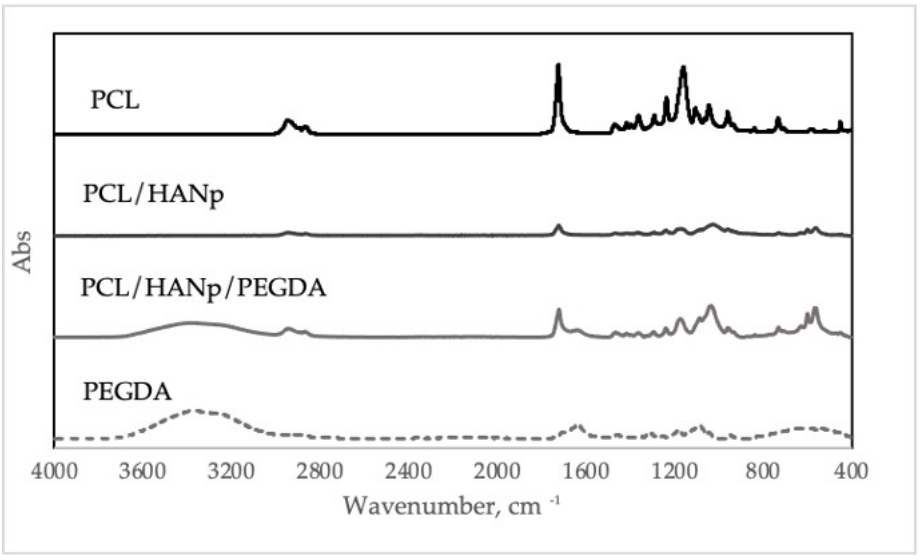

Figure 3. FTIR spectra of each group (PCL, PCL/HANp, PCL/HANp/PEGDA and PEGDA).

The wetting tendency of the samples was assessed by measuring the contact angle and shown in Figure 4.

Preprints (www.preprints.org) | NOT PEER-REVIEWED | Posted: 28 October 2022 doi:10.20944/preprints202210.0436.v1

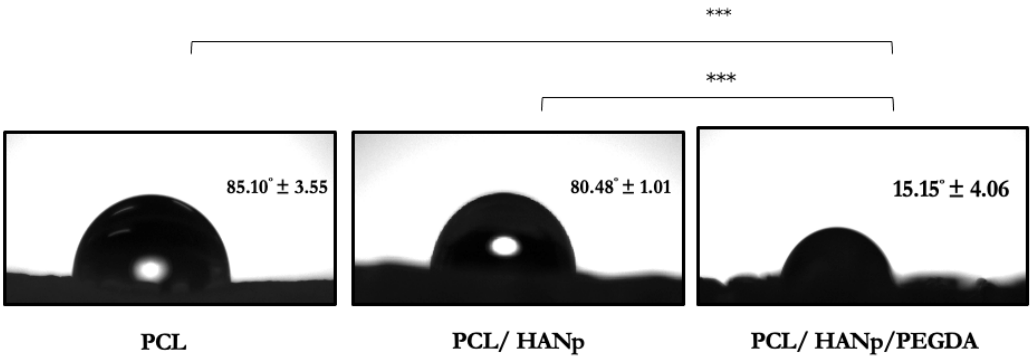

Figure 4. Contact angle measurements mean ± standard deviation of PCL, PCL/HANp and PCL/HANp/PEGDA scaffolds. Differences were considered statistically significant at $p \leq 0.05$. The results' significance is presented through the symbol (*), according to the p-value, with three symbols, corresponding to $0.0001 < p \leq 0.001$. .

This characterisation test revealed that the PCL scaffolds (85.10 ± 3.54°) presented a slightly higher contact angle than the PCL/HANp scaffolds (80.48 ± 1.01°). Nevertheless, the PCL/HANp/PEGDA group showed a significantly lower contact angle (15.15 ± 4.06°) than the other groups. Considering the results, the addition of HANp and PEGDA seems to have decreased the contact angle of the samples.

The internal and external morphologies (Figure 5) and the porosity (Table 1) of the scaffolds were studied by using X-ray micro-computed tomography.

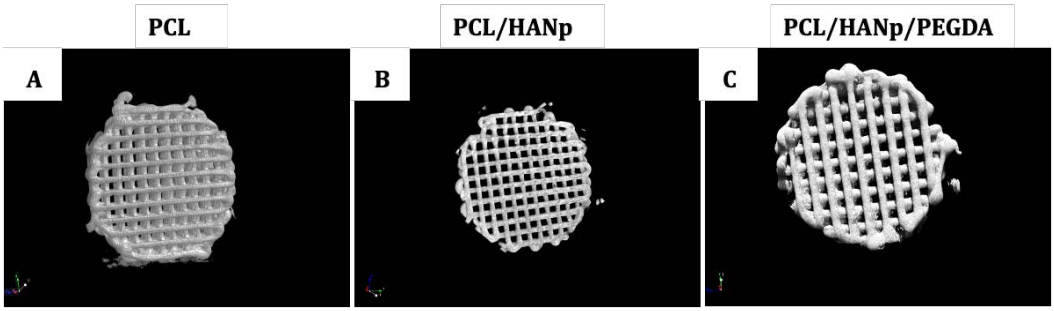

Figure 5. 3D micro-CT images of (a) PCL scaffolds; (b) PCL scaffolds with the addition of hydroxyapatite nanoparticles; (c) PCL/HANp scaffolds submerged in PEGDA solution.

Table 1. Porosity of PCL, PCL/HANp and PCL/HANp/PEGDA scaffolds (mean ± standard deviation). Differences were considered statistically significant at $p \leq 0.05$.

	PCL (1)	PCL/HANp (2)	PCL/HANp /PEGDA (3)	*p*
Porosity of scaffolds (%)	47.80 ± 0.90	52.20 ± 1.67	51.53 ± 2.00	(1) and (2) – 0.051 (1) and (3) – 0.065 (2) and (3) – 0.052

All scaffold groups were produced presenting interconnected channel networks and good geometric accuracy (Figure 4). Based on the results of porosity (%) of the scaffolds (Table 1), there is no evidence of significant statistical differences between the different scaffolds.

Concerning SEM analysis, it was used to visualise the filaments and pores of the prepared scaffolds, and details about their morphology and topography, as represented in Figure 6.

Preprints (www.preprints.org) | NOT PEER-REVIEWED | Posted: 28 October 2022 doi:10.20944/preprints202210.0436.v1

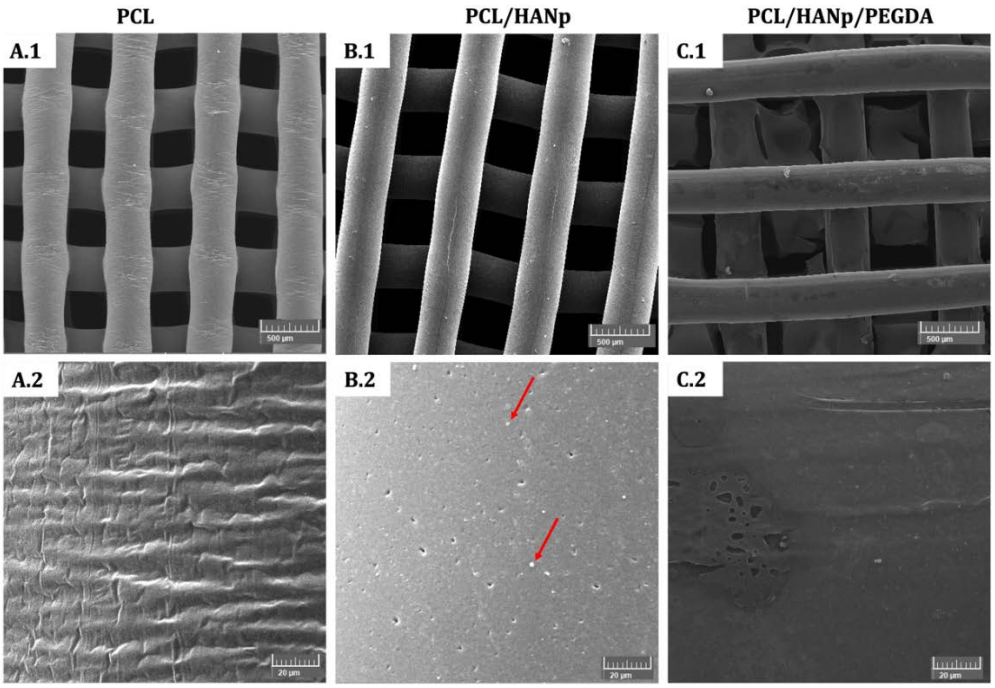

Figure 6. SEM images of PCL, PCL/HANp and PCL/HANp/PEGDA scaffolds. The red arrows show the presence of hydroxyapatite nanoparticles in the sample. Magnification: A.1, B.1 and C.1: 50x and, A.2, B.2 and C.2: 1000x.

According to the results, the scaffolds seem to have been successfully produced revealing interconnected porosity and well-accurate filaments. (Figure 6 A.1, B.1 and B.3). The structural characteristics of the scaffolds were also analysed by measuring the filaments and pore size for each experimental group. No statistical differences were found between the filaments of the three experimental groups. These measured approximately 400 μm in diameter, which corroborates with the conception parameters of the scaffolds. Furthermore, all scaffolds presented interconnected and square pores with diameters of 380 μm (with no statistical differences between the groups). At high magnifications, the PCL scaffolds revealed a filament surface with a small roughness (Figure 6 A.2). Already the PCL/HANp scaffold shows a flat filament surface with microporosities with a homogeneous dispersion in the matrix. It is also possible to distinguish small particles that suggest being hydroxyapatite nanoparticles (red arrows in Figure 6 B.2). Figure 6 C.2 displays a filament surface with a plasticised appearance and some roughness which is in line with the production of this scaffold as it was submerged in PEGDA. The hydrogel appears to be a well-distributed and uniform layer, although it appears to have small irregularities.

Additionally, EDX analysis was performed to determine the presence of individual elements and the calcium/phosphate molar ratio (Table 2).

Table 2. EDX analysis of the scaffolds produced and CA/P molar ratio results.

Scaffold	Oxygen (O)		Calcium (Ca)		Carbon (C)		Phosphorus (P)		Ca/P Molar Ratio
	Mass (%)	Atomic (%)	Mass (%)	Atomic (%)	Mass (%)	Atomic (%)	Mass (%)	Atomic (%)	
PCL	32.94	26.94	0.00	0.00	67.06	73.06	0.00	0.00	-
PCL/HANp	2.30	16.69	3.02	8.76	7.00	67.72	1.82	6.83	1.66
PCL/HANp/PEGDA	5.55	30.18	2.76	6.00	8.11	58.75	1.81	5.08	1.52

Preprints (www.preprints.org) | NOT PEER-REVIEWED | Posted: 28 October 2022 doi:10.20944/preprints202210.0436.v1

To demonstrate the homogeneous dispersion of HANp (composed of calcium and phosphate as previously mentioned) in the matrix, the PCL/HANp and PCL/HANp/PEGDA groups were observed by EDX Si mapping analyse, and the result is shown in Figure 7.

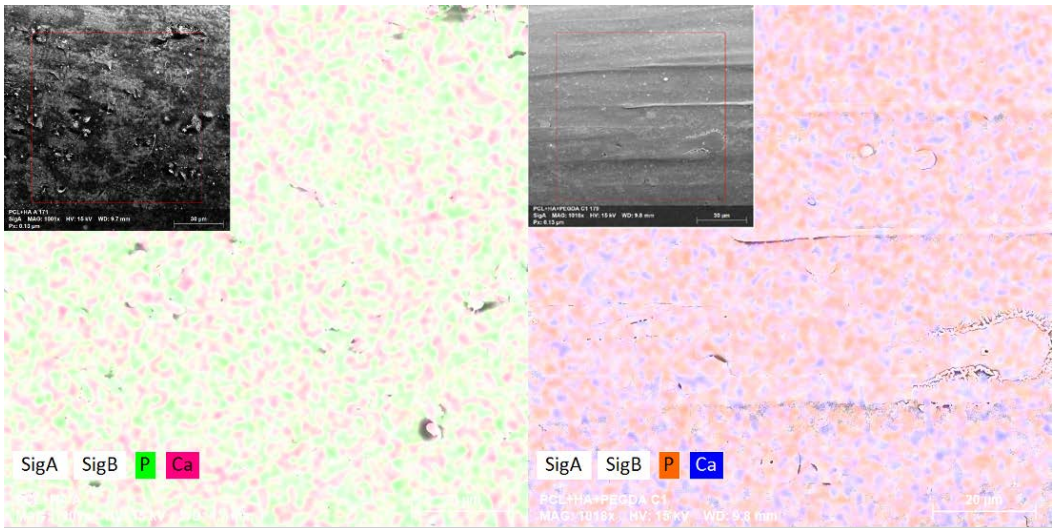

Figure 7. EDX Si-mapping micrographs.

Regarding mechanical behavior, compressive modulus (MPa) is reported in Figure 8 and Table 3. The mechanical behavior is mainly conditioned by the structural characteristics, such as pore size, pore wall and connection between pores. Although with no statistical differences, the PCL/HANp group presented a higher compression modulus compared to the PCL group. In contrast, the scaffolds with PEGDA showed a slight decrease in compression behaviour compared to the same group. Despite these results, the mechanical response of the three groups presented no statistically significant differences.

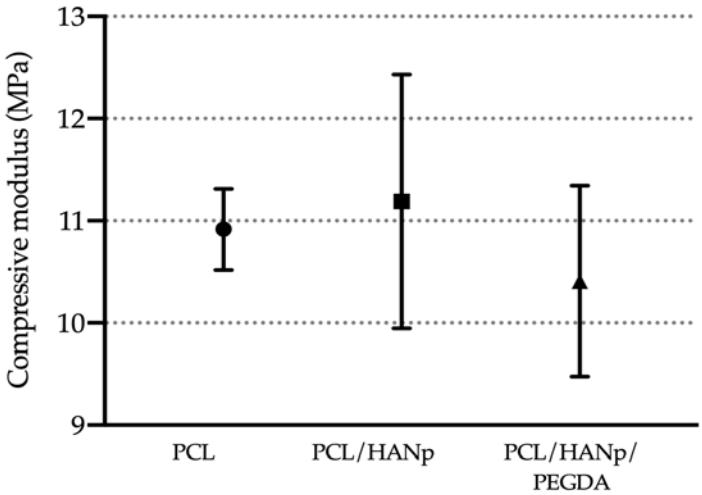

Figure 8. Compressive modulus (MPa) of the produced scaffolds.

Table 3. Compressive mechanical properties of the formulations produced (mean±sd values).

Parameter (MPa)	PCL	PCL/HANp	PCL/HANp/PEGDA
Compressive modulus E	10.92 ± 0.3965	11.19 ± 1.244	10.41 ± 0.9344

Preprints (www.preprints.org) | NOT PEER-REVIEWED | Posted: 28 October 2022 doi:10.20944/preprints202210.0436.v1

3.3. In vitro cytocompatibility test

According to ISO 10993-5:2009 guidelines, the viability was determined using PrestoBlue™ on PCL (gold standard), PCL/HANP and PCL/HANP/PEGDA scaffolds in the presence of hDPSCs. Figure 9 and Table 5 represent the corrected absorbance values for each time-point: 24, 72, 120, and 168 hours. Furthermore, the statistical differences identified between the experimental groups at each time-point are shown in Table 5.

The analysis results demonstrated in all groups a normal cell proliferation and growth rate until 120 hours, followed by a pronounced decrease in cell viability at 168 hours. Although the scaffolds with PCL/HANP presented slightly higher cell viability rates when compared with the PCL group, only at 120 hours statistically significant differences were identified. Conversely, PEGDA scaffolds demonstrated significantly higher absorbance than the standard group, suggesting evidence of induction of cell adhesion and proliferation. The PCL/HANp/PEGDA scaffolds presented overall a superior cytocompatibility performance, when in comparison with the gold standard PCL group.

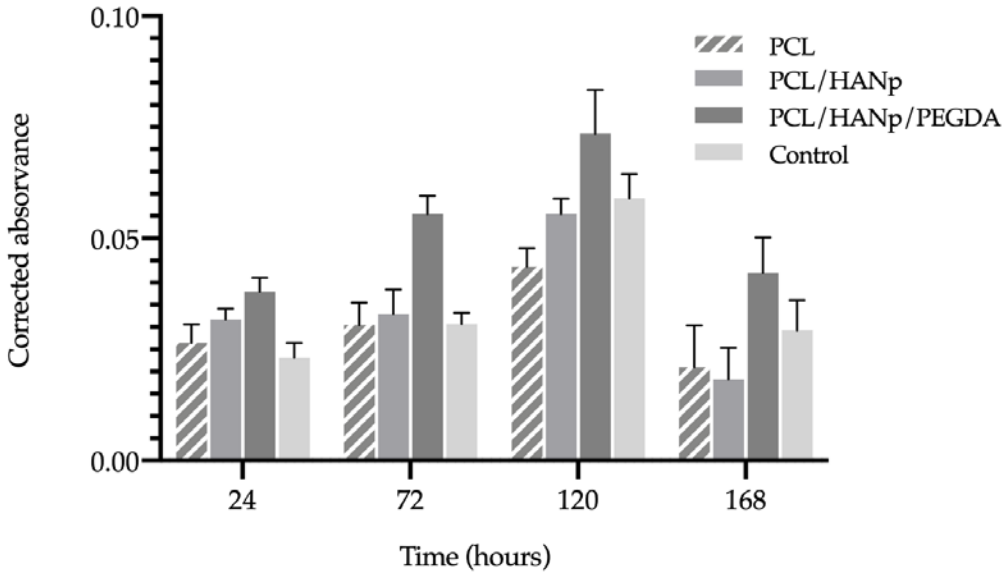

Figure 9. Corrected absorbance evaluated by PrestoBlue® viability assay for hDPSCs after 24, 72, 120 and 168 hours.

Table 4. Statistical significance of viability assay for hDPSCs after 24, 72, 120 and 168 hours (CT – control; ns - not significant). Results significances are presented through the symbol (*), according to the P value, with one, two, three or four symbols, corresponding to 0,01 < P ≤ 0,05; 0,001 < P 0,01; 0,0001 < P ≤ 0,001 and P ≤ 0,0001, respectively.

	24h				72h				120h				168h			
	PCL	PCL/ HANp	PCL/HANp/ PEGDA	CT	PCL	PCL/ HANp	PCL/HANp/ PEGDA	CT	PCL	PCL/ HANp	PCL/HANp/ PEGDA	CT	PCL	PCL/ HANP	PCL/HANp/ PEGDA	CT
PCL		ns	*	ns		ns	****	ns		*	****	**		ns	****	ns
PCL/HANp			ns	ns			****	ns			***	ns			****	*
PCL/HANp/PEGDA				**				****				**				*
CT																

Table 5. Corrected absorbance evaluated by PrestoBlue® viability assay for hDPSCs after 24, 72, 120 and 168 hours. Results presented in Mean ± SE.

	PCL	PCL/HANp	PCL/HANp/PEGDA	Control
24 h	0.027 ± 0.004	0.032 ± 0.002	0.038 ± 0.003	0.023 ± 0.003
72 h	0.031 ± 0.004	0.033 ± 0.005	0.056 ± 0.004	0.031 ± 0.002

Preprints (www.preprints.org) | NOT PEER-REVIEWED | Posted: 28 October 2022 doi:10.20944/preprints202210.0436.v1

120 h	0.044 ± 0.004	0.056 ± 0.003	0.074 ± 0.009	0.059 ± 0.005
168 h	0.021 ± 0.008	0.018 ± 0.006	0.042 ± 0.007	0.029 ± 0.006

The results of the percentage of viability inhibition, normalized to the PCL group (gold standard), are presented in Figure 10 and Table 6. In accordance with Annex 3 of the ISO 10993-5:2009 guideline, inhibition of viability when superior to 30% is considered a cytotoxic effect (represented in Figure 10 by dashed lines).

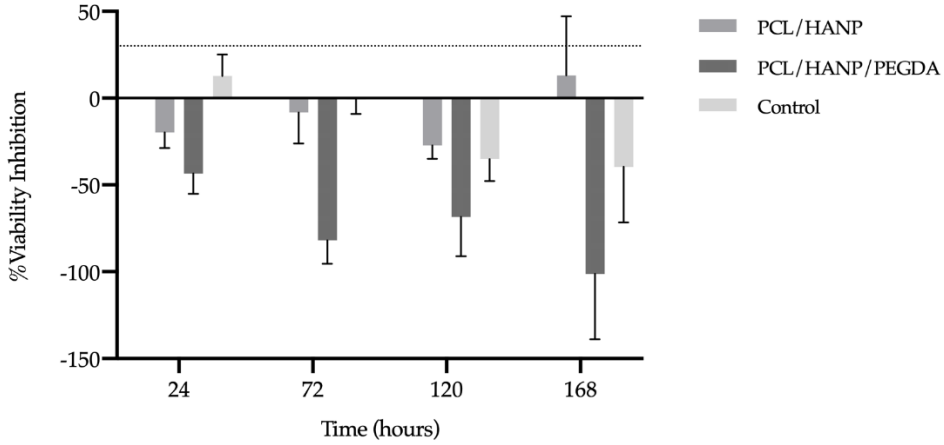

Figure 10. % Viability inhibition evaluated by PrestoBlue® viability assay for hDPSCs after 24, 72, 120 and 168 hours. Results are normalized to the PCL as 0%. The 30% threshold shown in the graph (dashed line) represents the inhibition above which the effect is considered cytotoxic (in accordance with ISO 10993-5:2009 guidelines). .

Table 6. % Viability inhibition evaluated by PrestoBlue® viability assay for hDPSCs after 24, 72, 120 and 168 hours. Results presented in Mean ± SE.

	PCL/HANp	PCL/HANp/PEGDA	Control
24 h	-19.81 ± 7.72	-43.40 ± 10.16	12.72 ± 10.77
72 h	-8.20 ± 15.47	-81.97 ± 11.59	-0.82 ± 10.10
120 h	-27.22 ± 6.68	-68.48 ± 19.62	-35.13 ± 10.87
168 h	13.10 ± 29.43	-101.19 ± 32.71	-39.52 ± 27.76

The results of the percentage of viability inhibition suggest that PCL/HANP and PCL/HANP/PEGDA scaffolds can be classified as non-cytotoxic, since the percentage of viability inhibition did not exceed the pre-established limit of 30%, according to the previously mentioned guideline.

4. Discussion

Additive manufacturing has emerged as an innovative approach to scaffold fabrication for regeneration of critical bone defects [64]. The most widely used addictive manufacturing technique is extrusion printing as it prints a wide variety of biomaterials at a low cost and with good precision [65]. In the present study, this technique allowed the printing of porous, biodegradable, and reproducible scaffolds, based on PCL, HANp and PEGDA, as a potential substitute for the treatment of bone defects. There are several reasons for the choice of PCL as the main component of the developed scaffolds. This thermoplastic polymer is widely used due to its biocompatibility, biodegradability, ease of processing (with a melting point between 55 and 60°C), with non-toxic degradation, and adjustable composition/structure [32-34,66-69]. Nevertheless, PCL presents some inconveniences such as low adhesion and cell proliferation and its slow degradation rate given the high degree of crystallinity and hydrophobicity [70,71]. These disadvantages can be

 doi:10.20944/preprints202210.0436.v1

overcome with the inclusion of specific compounds as inorganic bioactive materials, namely, calcium phosphates [72-74]. In this sense, hydroxyapatite nanoparticles were incorporated, thus improving the bioactivity, osteoconductivity, and hydrophilicity of the scaffold. Moreover, this inorganic component also tends to enhance the mechanical properties of the material [69,75]. The amount of HANp was set at 40% of the final weight of the composite, as higher proportions formed a mixture that was excessively thick, leading to clogging of the nozzle and non-uniform printing of the filaments. The incorporation of HANp in the PCL matrix was performed by solvent casting technique. This technique was used because it is simple and allows the control of porosity, pore size and interconnectivity [76]. After thefabrication of the scaffolds using the extrusion-based technique, they were further submerged in a PEGDA solution to promote cell adhesion, proliferation, and migration of the composite [49]. Although there are already several notable works on PCL/HANp scaffolds [23-26,29,47,51,77-81] with promising results, in reviewing the literature, no data were found on the potential of the association of these materials with PEGDA hydrogel to be used in bone defects to improve and accelerate bone regeneration. Therefore, the purpose of this study was the production, optimization, characterisation, and *in vitro* evaluation of three different matrices: i) PCL scaffolds; ii) PCL scaffolds with added HANp; and iii) PCL/HANp scaffolds submerged in PEGDA solution. It is relevant to highlight that all scaffolds were produced successfully and demonstrated good reproducibility (Figure 2).

Regarding the FTIR spectroscopy analysis, it was possible to detect the functional groups in the respective samples (Figure 3). The spectra of the scaffold groups presented the respective characteristic absorption bands of PCL, HANp and PEGDA and are following the literature [60-63].

The wetting of the material was analysed by the contact angle of the samples for the different groups (Figure 4). The porous structure of the scaffolds did not allow a correct measurement of the angles. For this reason, flat segments of each composite were used for more precise measurement. Regarding the results of the contact angle measurement, it can be inferred that the PCL surface had a higher contact angle, supporting a hydrophobic nature [82,83]. Nevertheless, the addition of HANp to PCL slightly decreased the contact angle and therefore increased the wettability of the composite surface. These results are in agreement with the literature and are explained by the hydrophilic nature of hydroxyapatite [84,85]. Meanwhile, the PCL/HANp/PEGDA group demonstrated a significantly lower contact angle than the other groups. This is explained by the hydrophilic nature of the PEGDA hydrogel [49]. The addition of HANp and PEGDA may thus enhance cell activity, namely cell adhesion and proliferation, and therefore be a composite more suitable for bone tissue engineering.

To evaluate the internal and external morphology and porosity of the scaffolds, X-ray micro-computed tomography was performed (Figure 5 and Table 1). According to the results, the three groups of scaffolds were correctly produced, presenting good geometry accuracy, filaments according to the pre-established pattern and interconnected channel networks. The porosity percentage of the scaffolds was also calculated, which is defined as the percentage of void space in a solid, which is considered a material-independent property [86]. The calculated porosities of the scaffolds were approximately 50%, which is recognized as a valid value considering the literature [47,86]. The pores of the scaffolds allow the formation of bone tissue as they facilitate the migration and proliferation of osteoblasts. These structures also allow for adequate vascularization in the scaffolds [86]. Furthermore, the porous surfaces enhance mechanical interlocking at the interface between the scaffold and the surrounding bone, providing higher mechanical stability. The addition of PEGDA slightly decreased the porosity of the scaffolds, however, there is no evidence of statistically significant differences between the different scaffolds. Thus, it appears that regardless of the material, all structures had similar porosity values. These results support the reliability of the biomanufacturing system used in the production of the samples.

 doi:10.20944/preprints202210.0436.v1

SEM micrographs performed on the scaffolds revealed structures with a well-defined internal geometry with square and interconnected pores with regular dimensions and uniform distribution (Figure 6). The pores presented a size in the order of 380 µm. Studies have revealed that larger pores translate into higher mature bone formation and promote vascularization [87,88]. This phenomenon is explained by the formation of blood vessels that, by supplying oxygen and nutrients necessary for osteoblastic activity in the larger pores of the scaffolds, promote the formation of new bone mass [88,89]. The filaments also had a regular circular geometry approximately of 400µm in diameter, in agreement with the needle used (400µm). At high magnifications, a rough filament surface is visible on the PCL scaffold, in contrast to the PCL/HANp scaffold with a smoother surface, microporosities and homogeneously distributed hydroxyapatite nanoparticles. The addition of solvent (DMF) in the solvent casting method seems to promote microporosity and thus favour cell adhesion [26,90]. In turn, the PCL/HANp/PEGDA scaffold presents a uniform layer with small irregularities.

Concerning EDX (Table 2) quantification the presence of a considerable amount of Oxygen and Carbon atoms is noticeable in all samples, which was closely related to the composition of the PCL polymer matrix [91]. Moreover, the elemental composition analysis of the PCL/HANp and PCL/HANp/PEGDA groups also indicates significant amounts of Calcium and Phosphorus, which are the basic elements of the hydroxyapatite ceramic ($Ca_{10}(PO_4)_6(OH)_2$)[92]. In contrast, the PCL scaffold no longer shows concentrations of these chemical elements, as would be expected. EDX Ca/P determination was performed to the fabricated scaffolds, confirming the formation of CaP in the PCL/HANp and PCL/HANp/PEGDA scaffolds. The Ca/P molar ratio measured in these groups is similar to the stoichiometric value of HAp (1.67) [93]. As illustrated in the EDX Si mapping micrographs (Fig. 7), HANp (constituted by Calcium and Phosphorus) seems to be homogeneously distributed in the PCL matrix in the experimental groups of PCL/HANp and PCL/HANp/PEGDA. These data are following the SEM analysis results.

The values of the compressive modulus obtained for all scaffold groups are presented in Figure 8 and Table 3. The PCL/HANp group and the PCL/HANp/PEGDA group presented slightly higher and lower compression modulus, respectively, when compared to the PCL group. These results may be explained by the higher strength and stiffness properties associated with HANp [94,95]. In turn, PEGDA is considered a hydrogel and therefore when incorporated into the scaffold a decrease in compression modulus would be expected [42]. Notwithstanding, the average compression modulus of the three groups did not present statistically significant differences. The mechanical behaviour is mainly conditioned by structural features, such as porosity, pore size, and interconnectivity. Therefore, these results are in line with previously presented results on SEM micrographs and X-ray micro-computed tomography since the values of porosity/pore size/interconnectivity are very similar in all the produced scaffolds. Overall, the results of the mechanical behaviour demonstrated that the produced scaffolds fulfil the minimum compressive modulus required for bone graft substitutes, as it is superior to 0.5 MPa [42,96]. It should be noted that the compressive strength of the structures produced is within the range of values for human cancellous bone, from 5 to 50 MPa (depending on bone density) [97].

The cell viability and proliferation of hDPSCs in contact with the scaffolds was investigated by PrestoBlue™ (Figure 9 and Table 4). This test was performed according to ISO 10993-5:2009 "Biological evaluation of medical devices-Part 5-Test for *in vitro* cytotoxicity". The cells used in this assay were hDPSCs given their proven potential for osteogenic lineage and consequent suitability for bone tissue regeneration [1,98,99]. Moreover, in the literature there are other works that successfully assess the cytocompatibility of PCL and PCL/HANp scaffolds with this cell lineage [51,100-104]. The viability of the control group (without scaffolds) demonstrated a normal cell proliferation and growth rate, thus confirming the validity of this assay. According to Figure 9, the absorbance increased until the 5th day of cell culture, for all experimental conditions. However, on the 7th day of culture it is noticeable that all experimental groups presented a decreased cell viability. It can be hypothesised that cells on the 7th day are in the decline/apoptosis phase due to

 doi:10.20944/preprints202210.0436.v1

competitive inhibition resulting from the excess of cells in each well. During the cell death phase occurs the irreversible loss of cell division capacity (cell death) is triggered by the considerable increase in intracellular calcium concentration ($[Ca^{2+}]_i$). At 24, 72 and 120 hours of incubation, the PCL/HANp group showed a higher viability value (only at 120 hours $p<0.05$) compared to the PCL scaffolds group. The fact that HANP is considered a bioactive, osteoconductive and hydrophilic material may contribute to these results [69,75]. In addition, the PrestoBlue™ viability assay demonstrated that the PCL/HANp/PEGDA scaffolds showed overall superior cytocompatibility performance compared with the gold standard PCL scaffold. The improved cytocompatibility results thus tend to be associated with the PEGDA hydrogel, as it has been supported by other groups working with this same material [42,105-107]. In sum, the results of the *in vitro* evaluation led to the assumption that the addition of PEGDA promoted cell migration and proliferation. According to Figure 10 and Table 6, all experimental groups can be classified as non-cytotoxic, as the % viability inhibition did not exceed the pre-established 30% limit throughout the test, according to the ISO 10993-5:2009 guideline.

5. Conclusions

This study describes the production, characterisation and *in vitro* performance of a scaffold based on PCL, HANp and PEGDA for bone application. Thus far, there is a wealth of literature proposing the use of PCL as a scaffold for bone pathologies. Nevertheless, to the best of our knowledge, this is the first study incorporating PCL, HANp and PEGDA in a scaffold for the healing of critical defects.

The characterisation revealed that scaffolds were successfully produced, with well-coordinated and positioned filaments, interconnected channels, and pores propitious to the migration and proliferation of osteoblasts and stem cells. Moreover, the scaffolds with PEGDA demonstrated to have hydrophilic properties that can also favour cellular activity, without compromising the mechanical properties of the composite. The results of the in *vitro* test are consistent with previously demonstrated results with a superior proliferation of hDPSCs in the PEGDA groups.

According to the results, PCL/HANp/PEGDA scaffolds are a very promising therapeutic system in critical fracture treatment, to accelerate and improve bone regeneration. The research on this system's performance in critical bone defects is an important step in its progression to clinical applications.

Author Contributions: Conceptualization, A.C.S., S.B, N.A. and A.C.M.; methodology, A.C.S., S.B., J.F.A.V. and M.F.; software, A.C.S., S.B., J.F.A.V. and M.F.; validation, A.C.S, S.B., R.A. M.B., B.L., P.S., J.F.A.V. and M.F.; formal analysis, A.C.S.; investigation, A.C.S., S.B., N.A. and A.C.M..; resources, N.A. and A.C.M; data curation, A.C.S.; writing—original draft preparation, A.C.S.; writing—review and editing, A.C.S.; visualization, A.C.S, S.B., R.A. M.B., B.L., P.S., J.F.A.V., M.F., L.A., J.D.S., N.A. and A.C.M.; supervision, L.A., J.D.S., N.A. and A.C.M; project administration, N.A. and A.C.M..; funding acquisition, N.A. and A.C.M. . All authors have read and agreed to the published version of the manuscript.

Funding: Mariana Vieira Branquinho (SFRH/BD/146172/2019), Ana Catarina Sousa (SFRH/BD/146689/2019), and Bruna Lopes (2021.05265.BD), acknowledge Fundação para a Ciência e Tecnologia (FCT), for financial support. Rui Damásio Alvites acknowledges the Animal Science Studies Centre (CECA), Agroenvironment, Technologies and Sciences Institute (ICETA), Porto University (UP), and FCT for the funding and availability of all technical, structural, and human resources necessary for the development of this work. This research was funded by Projects PEst-OE/AGR/UI0211/2011 from FCT, and COMPETE 2020, from ANI–Projetos ID&T Empresas em Copromoção, by the project "Print-on-Organs–Engineering bioinks and processes for direct printing on organs" with the reference POCI-01-0247-FEDER-033877, by the project "Bone2Move-Development of "in vivo" experimental techniques and modelling methodologies for the evaluation of 4D scaffolds for bone defect in sheep model: an integrative research approach" with the reference POCI-01-0145-FEDER-031146. This work was also supported by the Fundação para a Ciência e a Tecnologia (FCT) and Centro2020 through the following Projects: UIDB/04044/2020, UIDP/04044/2020, and PAMI—ROTEIRO/0328/2013 (Nº 022158).

Institutional Review Board Statement: Not applicable.

Data Availability Statement: Further data on the reported results are available from the corresponding author on request.

Acknowledgments: Not applicable.

Conflicts of Interest: The authors declare no conflict of interest.

References

1. Campos, J.M.; Sousa, A.C.; Caseiro, A.R.; Pedrosa, S.S.; Pinto, P.O.; Branquinho, M.V.; Amorim, I.; Santos, J.D.; Pereira, T.; Mendonça, C.M.; et al. Dental pulp stem cells and Bonelike(®) for bone regeneration in ovine model. *Regen Biomater* **2019**, *6*, 49-59, doi:10.1093/rb/rby025.
2. Bohner, M. Resorbable biomaterials as bone graft substitutes. *Materials Today* **2010**, *13*, 24-30, doi:10.1016/S1369-7021(10)70014-6.
3. Forrestal, D.P.; Klein, T.J.; Woodruff, M.A. Challenges in engineering large customized bone constructs. *Biotechnology and bioengineering* **2017**, *114*, 1129-1139.
4. Bahraminasab, M. Challenges on optimization of 3D-printed bone scaffolds. *BioMedical Engineering OnLine* **2020**, *19*, 69, doi:10.1186/s12938-020-00810-2.
5. Lopes, B.; Sousa, P.; Alvites, R.; Branquinho, M.; Sousa, A.C.; Mendonça, C.; Atayde, L.M.; Luís, A.L.; Varejão, A.S.P.; Maurício, A.C. Peripheral Nerve Injury Treatments and Advances: One Health Perspective. *Int J Mol Sci* **2022**, *23*, doi:10.3390/ijms23020918.
6. Shang, F.; Yu, Y.; Liu, S.; Ming, L.; Zhang, Y.; Zhou, Z.; Zhao, J.; Jin, Y. Advancing application of mesenchymal stem cell-based bone tissue regeneration. *Bioactive Materials* **2021**, *6*, 666-683, doi:https://doi.org/10.1016/j.bioactmat.2020.08.014.
7. Visser, J.; Melchels, F.P.; Jeon, J.E.; Van Bussel, E.M.; Kimpton, L.S.; Byrne, H.M.; Dhert, W.J.; Dalton, P.D.; Hutmacher, D.W.; Malda, J. Reinforcement of hydrogels using three-dimensionally printed microfibres. *Nature communications* **2015**, *6*, 1-10.
8. Woodfield, T.; Lim, K.; Morouço, P.; Levato, R.; Malda, J.; Melchels, F. Biofabrication in tissue engineering. In *Comprehensive Biomaterials II*, Ducheyne P. ed.; Elsevier, A., Ed.; 2017; pp. 236–266.
9. Bahraminasab, M.; Edwards, K. Biocomposites for Hard Tissue Replacement and Repair. 2018; pp. 281-296.
10. Kohn, J. New approaches to biomaterials design. *Nature materials* **2004**, *3*, 745-747.
11. Zhang, L.; Yang, G.; Johnson, B.N.; Jia, X. Three-dimensional (3D) printed scaffold and material selection for bone repair. *Acta Biomaterialia* **2019**, *84*, 16-33, doi:https://doi.org/10.1016/j.actbio.2018.11.039.
12. Brown, B.N.; Valentin, J.E.; Stewart-Akers, A.M.; McCabe, G.P.; Badylak, S.F. Macrophage phenotype and remodeling outcomes in response to biologic scaffolds with and without a cellular component. *Biomaterials* **2009**, *30*, 1482-1491.
13. Porter, J.R.; Ruckh, T.T.; Popat, K.C. Bone tissue engineering: a review in bone biomimetics and drug delivery strategies. *Biotechnol Prog* **2009**, *25*, 1539-1560, doi:10.1002/btpr.246.
14. Ghassemi, T.; Shahroodi, A.; Ebrahimzadeh, M.H.; Mousavian, A.; Movaffagh, J.; Moradi, A. Current Concepts in Scaffolding for Bone Tissue Engineering. *Arch Bone Jt Surg* **2018**, *6*, 90-99.
15. Qu, H.; Fu, H.; Han, Z.; Sun, Y. Biomaterials for bone tissue engineering scaffolds: a review. *RSC Adv* **2019**, *9*, 26252-26262, doi:10.1039/c9ra05214c.
16. Langer, R.; Vacanti, J.P. Tissue engineering. *Science* **1993**, *260*, 920, doi:10.1126/science.8493529.
17. Dominici, M.; Le Blanc, K.; Mueller, I.; Slaper-Cortenbach, I.; Marini, F.C.; Krause, D.S.; Deans, R.J.; Keating, A.; Prockop, D.J.; Horwitz, E.M. Minimal criteria for defining multipotent mesenchymal stromal cells. The International Society for Cellular Therapy position statement. *Cytotherapy* **2006**, *8*, 315-317, doi:https://doi.org/10.1080/14653240600855905.
18. Lawson, A.C.; Czernuszka, J.T. Collagen-calcium phosphate composites. *Proceedings of the Institution of Mechanical Engineers, Part H: Journal of Engineering in Medicine* **1998**, *212*, 413-425, doi:10.1243/0954411981534187.
19. Jensen, S.S.; Broggini, N.; Hjørting-Hansen, E.; Schenk, R.; Buser, D. Bone healing and graft resorption of autograft, anorganic bovine bone and β-tricalcium phosphate. A histologic and histomorphometric study in the mandibles of minipigs. *Clinical Oral Implants Research* **2006**, *17*, 237-243, doi:https://doi.org/10.1111/j.1600-0501.2005.01257.x.
20. Jensen, S.S.; Yeo, A.; Dard, M.; Hunziker, E.; Schenk, R.; Buser, D. Evaluation of a novel biphasic calcium phosphate in standardized bone defects. A histologic and histomorphometric study in the mandibles of minipigs. *Clinical Oral Implants Research* **2007**, *18*, 752-760, doi:https://doi.org/10.1111/j.1600-0501.2007.01417.x.
21. Kattimani, V.S.; Kondaka, S.; Lingamaneni, K.P. Hydroxyapatite–-Past, Present, and Future in Bone Regeneration. *Bone and Tissue Regeneration Insights* **2016**, *7*, BTRI.S36138, doi:10.4137/btri.S36138.
22. Song, H.H.; Yoo, M.K.; Moon, H.S.; Choi, Y.J.; Lee, H.C.; Cho, C.S. A novel polycaprolactone/hydroxyapatite scaffold for bone tissue engineering. In Proceedings of the Key Engineering Materials, 2007; pp. 265-268.
23. Zhao, J.; Guo, L.; Yang, X.; Weng, J. Preparation of bioactive porous HA/PCL composite scaffolds. *Applied Surface Science* **2008**, *255*, 2942-2946.
24. Park, S.A.; Lee, S.H.; Kim, W.D. Fabrication of porous polycaprolactone/hydroxyapatite (PCL/HA) blend scaffolds using a 3D plotting system for bone tissue engineering. *Bioprocess and biosystems engineering* **2011**, *34*, 505-513.
25. Zimmerling, A.; Yazdanpanah, Z.; Cooper, D.M.L.; Johnston, J.D.; Chen, X. 3D printing PCL/nHA bone scaffolds: exploring the influence of material synthesis techniques. *Biomaterials Research* **2021**, *25*, 3, doi:10.1186/s40824-021-00204-y.

26. Cestari, F.; Petretta, M.; Yang, Y.; Motta, A.; Grigolo, B.; Sglavo, V.M. 3D printing of PCL/nano-hydroxyapatite scaffolds derived from biogenic sources for bone tissue engineering. *Sustainable Materials and Technologies* **2021**, *29*, e00318, doi:https://doi.org/10.1016/j.susmat.2021.e00318.
27. Zhao, J.; Duan, K.; Zhang, J.W.; Lu, X.; Weng, J. The influence of polymer concentrations on the structure and mechanical properties of porous polycaprolactone-coated hydroxyapatite scaffolds. *Applied Surface Science* **2010**, *256*, 4586-4590, doi:https://doi.org/10.1016/j.apsusc.2010.02.053.
28. Jirkovec, R.; Holec, P.; Hauzerova, S.; Samkova, A.; Kalous, T.; Chvojka, J. Preparation of a Composite Scaffold from Polycaprolactone and Hydroxyapatite Particles by Means of Alternating Current Electrospinning. *ACS Omega* **2021**, *6*, 9234-9242, doi:10.1021/acsomega.1c00644.
29. Shor, L.; Güçeri, S.; Wen, X.; Gandhi, M.; Sun, W. Fabrication of three-dimensional polycaprolactone/hydroxyapatite tissue scaffolds and osteoblast-scaffold interactions in vitro. *Biomaterials* **2007**, *28*, 5291-5297.
30. Cho, Y.S.; Gwak, S.-J.; Cho, Y.-S. Fabrication of Polycaprolactone/Nano Hydroxyapatite (PCL/nHA) 3D Scaffold with Enhanced In Vitro Cell Response via Design for Additive Manufacturing (DfAM). *Polymers* **2021**, *13*, 1394.
31. Chuenjitkuntaworn, B.; Osathanon, T.; Nowwarote, N.; Supaphol, P.; Pavasant, P. The efficacy of polycaprolactone/hydroxyapatite scaffold in combination with mesenchymal stem cells for bone tissue engineering. *Journal of Biomedical Materials Research Part A* **2016**, *104*, 264-271, doi:https://doi.org/10.1002/jbm.a.35558.
32. Wang, S.; Gu, R.; Wang, F.; Zhao, X.; Yang, F.; Xu, Y.; Yan, F.; Zhu, Y.; Xia, D.; Liu, Y. 3D-Printed PCL/Zn scaffolds for bone regeneration with a dose-dependent effect on osteogenesis and osteoclastogenesis. *Materials Today Bio* **2022**, *13*, 100202, doi:https://doi.org/10.1016/j.mtbio.2021.100202.
33. Babilotte, J.; Guduric, V.; Le Nihouannen, D.; Naveau, A.; Fricain, J.-C.; Catros, S. 3D printed polymer–mineral composite biomaterials for bone tissue engineering: Fabrication and characterization. *Journal of Biomedical Materials Research Part B: Applied Biomaterials* **2019**, *107*, 2579-2595, doi:https://doi.org/10.1002/jbm.b.34348.
34. Kenry; Liu, B. Recent Advances in Biodegradable Conducting Polymers and Their Biomedical Applications. *Biomacromolecules* **2018**, *19*, 1783-1803, doi:10.1021/acs.biomac.8b00275.
35. Zhang, S.; Liu, C. Research progress in osteogenic differentiation of adipose-derived stem cells induced by bioscaffold materials. *Chinese Journal of Tissue Engineering Research* **2020**, *24*, 1107.
36. Patel, P.P.; Buckley, C.; Taylor, B.L.; Sahyoun, C.C.; Patel, S.D.; Mont, A.J.; Mai, L.; Patel, S.; Freeman, J.W. Mechanical and biological evaluation of a hydroxyapatite-reinforced scaffold for bone regeneration. *Journal of Biomedical Materials Research Part A* **2019**, *107*, 732-741, doi:https://doi.org/10.1002/jbm.a.36588.
37. Bal, Z.; Kaito, T.; Korkusuz, F.; Yoshikawa, H. Bone regeneration with hydroxyapatite-based biomaterials. *Emergent Materials* **2020**, *3*, 521-544, doi:10.1007/s42247-019-00063-3.
38. Wang, Y.; Cao, X.; Ma, M.; Lu, W.; Zhang, B.; Guo, Y. A GelMA-PEGDA-nHA Composite Hydrogel for Bone Tissue Engineering. *Materials (Basel)* **2020**, *13*, doi:10.3390/ma13173735.
39. Liu, W.; Jing, X.; Xu, Z.; Teng, C. PEGDA/HA mineralized hydrogel loaded with Exendin4 promotes bone regeneration in rat models with bone defects by inducing osteogenesis. *Journal of Biomaterials Applications* **2021**, *35*, 1337-1346, doi:10.1177/0885328220987046.
40. Martin, V.; Bettencourt, A. Bone regeneration: Biomaterials as local delivery systems with improved osteoinductive properties. *Materials Science and Engineering: C* **2018**, *82*, 363-371, doi:https://doi.org/10.1016/j.msec.2017.04.038.
41. Thrivikraman, G.; Athirasala, A.; Twohig, C.; Boda, S.K.; Bertassoni, L.E. Biomaterials for craniofacial bone regeneration. *Dental Clinics* **2017**, *61*, 835-856.
42. Kotturi, H.; Abuabed, A.; Zafar, H.; Sawyer, E.; Pallipparambil, B.; Jamadagni, H.; Khandaker, M. Evaluation of Polyethylene Glycol Diacrylate-Polycaprolactone Scaffolds for Tissue Engineering Applications. *J Funct Biomater* **2017**, *8*, doi:10.3390/jfb8030039.
43. Yang, F.; Williams, C.G.; Wang, D.A.; Lee, H.; Manson, P.N.; Elisseeff, J. The effect of incorporating RGD adhesive peptide in polyethylene glycol diacrylate hydrogel on osteogenesis of bone marrow stromal cells. *Biomaterials* **2005**, *26*, 5991-5998, doi:10.1016/j.biomaterials.2005.03.018.
44. Guarino, V.; Gloria, A.; Raucci, M.; Ambrosio, L. Hydrogel-Based Platforms for the Regeneration of Osteochondral Tissue and Intervertebral Disc. *Polymers* **2012**, *4*, 1590-1612, doi:10.3390/polym4031590.
45. Yang, Y.; Wang, G.; Liang, H.; Gao, C.; Peng, S.; Shen, L.; Shuai, C. Additive manufacturing of bone scaffolds. *Int J Bioprint* **2019**, *5*, 148, doi:10.18063/IJB.v5i1.148.
46. Sa, M.W.; Nguyen, B.B.; Moriarty, R.A.; Kamalitdinov, T.; Fisher, J.P.; Kim, J.Y. Fabrication and evaluation of 3D printed BCP scaffolds reinforced with ZrO(2) for bone tissue applications. *Biotechnol Bioeng* **2018**, *115*, 989-999, doi:10.1002/bit.26514.
47. Morouço, P.; Biscaia, S.; Viana, T.; Franco, M.; Malça, C.; Mateus, A.; Moura, C.; Ferreira, F.C.; Mitchell, G.; Alves, N.M. Fabrication of Poly(ε-caprolactone) Scaffolds Reinforced with Cellulose Nanofibers, with and without the Addition of Hydroxyapatite Nanoparticles. *Biomed Res Int* **2016**, *2016*, 1596157, doi:10.1155/2016/1596157.
48. Biscaia, S.; Dabrowska, E.; Tojeira, A.; Horta, J.; Carreira, P.; Morouço, P.; Mateus, A.; Alves, N. Development of heterogeneous structures with Polycaprolactone-Alginate using a new 3D printing system–BioMEDβeta: design and processing. *Procedia Manufacturing* **2017**, *12*, 113-119.
49. Francisco, L.; Moura, C.; Viana, T.; Ângelo, D.; Morouço, P.; Alves, N. Poly(ε-caprolactone) and Polyethylene Glycol Diacrylate-based Scaffolds for TMJ Bioengineered Disc Implants. *Procedia Manufacturing* **2017**, *12*, 291-297, doi:https://doi.org/10.1016/j.promfg.2017.08.032.

50. Moura, C.; Trindade, D.; Vieira, M.; Francisco, L.; Ângelo, D.F.; Alves, N. Multi-Material Implants for Temporomandibular Joint Disc Repair: Tailored Additive Manufacturing Production. *Front Bioeng Biotechnol* **2020**, *8*, 342, doi:10.3389/fbioe.2020.00342.
51. Biscaia, S.; Branquinho, M.V.; Alvites, R.D.; Fonseca, R.; Sousa, A.C.; Pedrosa, S.S.; Caseiro, A.R.; Guedes, F.; Patrício, T.; Viana, T.; et al. 3D Printed Poly(ε-caprolactone)/Hydroxyapatite Scaffolds for Bone Tissue Engineering: A Comparative Study on a Composite Preparation by Melt Blending or Solvent Casting Techniques and the Influence of Bioceramic Content on Scaffold Propertie. *Int J Mol Sci* **2022**, *23*, 2318.
52. Domingos, M.; Intranuovo, F.; Russo, T.; De Santis, R.; Gloria, A.; Ambrosio, L.; Ciurana, J.; Bartolo, P. The first systematic analysis of 3D rapid prototyped poly(ε-caprolactone) scaffolds manufactured through BioCell printing: the effect of pore size and geometry on compressive mechanical behaviour and in vitro hMSC viability. *Biofabrication* **2013**, *5*, 045004, doi:10.1088/1758-5082/5/4/045004.
53. Domingos, M.; Intranuovo, F.; Gloria, A.; Gristina, R.; Ambrosio, L.; Bártolo, P.J.; Favia, P. Improved osteoblast cell affinity on plasma-modified 3-D extruded PCL scaffolds. *Acta Biomaterialia* **2013**, *9*, 5997-6005, doi:https://doi.org/10.1016/j.actbio.2012.12.031.
54. Bartolo, P.; Domingos, M.; Gloria, A.; Ciurana, J. BioCell Printing: Integrated automated assembly system for tissue engineering constructs. *CIRP Annals* **2011**, *60*, 271-274, doi:https://doi.org/10.1016/j.cirp.2011.03.116.
55. Ângelo, D.F.; Morouço, P.; Monje Gil, F.; Mónico, L.; González-Gárcia, R.; Sousa, R.; Neto, L.; Caldeira, I.; Smith, M.; Smith, S.; et al. Preclinical randomized controlled trial of bilateral discectomy versus bilateral discopexy in Black Merino sheep temporomandibular joint: TEMPOJIMS – Phase 1- histologic, imaging and body weight results. *Journal of Cranio-Maxillofacial Surgery* **2018**, *46*, 688-696, doi:https://doi.org/10.1016/j.jcms.2018.01.006.
56. Viana, T.; Biscaia, S.; Dabrowska, E.; Franco, M.C.; Carreira, P.; Morouço, P.; Alves, N. A Novel Biomanufacturing System to Produce Multi-Material Scaffolds for Tissue Engineering: Concept and Preliminary Results. *Applied Mechanics and Materials* **2019**, *890*, 283-289, doi:10.4028/www.scientific.net/AMM.890.283.
57. Domingos, M.; Dinucci, D.; Cometa, S.; Alderighi, M.; Bártolo, P.J.; Chiellini, F. Polycaprolactone Scaffolds Fabricated via Bioextrusion for Tissue Engineering Applications. *International Journal of Biomaterials* **2009**, *2009*, 239643, doi:10.1155/2009/239643.
58. Morouço, P.; Ângelo, D.; Francisco, L.; Moura, C.; Alves, N. Tissue engineering for temporomandibular joint disc repair and regeneration: a methodological perspective. *Advances in Cellular and Molecular Otolaryngology* **2016**, *4*, 33709, doi:10.3402/acmo.v4.33709.
59. ThermoFisher. PrestoBlue™ Cell Viability Reagent. Available online: https://www.thermofisher.com/order/catalog/product/A13261 (accessed on
60. Lizarraga, K.; Flores-Morales, C.; Del Prado, M.; Álvarez-Pérez, M.; Pina-Barba, M.; Escobedo, C. Polycaprolactone- and polycaprolactone/ceramic-based 3D-bioplotted porous scaffolds for bone regeneration: A comparative study. *Materials Science and Engineering: C* **2017**, *79*, doi:10.1016/j.msec.2017.05.003.
61. Elzein, T.; Nasser-Eddine, M.; Delaite, C.; Bistac, S.; Dumas, P. FTIR study of polycaprolactone chain organization at interfaces. *Journal of Colloid and Interface Science* **2004**, *273*, 381-387, doi:https://doi.org/10.1016/j.jcis.2004.02.001.
62. Chang, M.C.; Tanaka, J. FT-IR study for hydroxyapatite/collagen nanocomposite cross-linked by glutaraldehyde. *Biomaterials* **2002**, *23*, 4811-4818, doi:10.1016/s0142-9612(02)00232-6.
63. Kianfar, P.; Vitale, A.; Dalle Vacche, S.; Bongiovanni, R. Enhancing properties and water resistance of PEO-based electrospun nanofibrous membranes by photo-crosslinking. *Journal of Materials Science* **2021**, *56*, 1-18, doi:10.1007/s10853-020-05346-3.
64. Do, A.V.; Khorsand, B.; Geary, S.M.; Salem, A.K. 3D Printing of Scaffolds for Tissue Regeneration Applications. *Adv Healthc Mater* **2015**, *4*, 1742-1762, doi:10.1002/adhm.201500168.
65. Garot, C.; Bettega, G.; Picart, C. Additive Manufacturing of Material Scaffolds for Bone Regeneration: Toward Application in the Clinics. *Advanced Functional Materials* **2021**, *31*, 2006967, doi:https://doi.org/10.1002/adfm.202006967.
66. Rohner, D.; Hutmacher, D.W.; Cheng, T.K.; Oberholzer, M.; Hammer, B. In vivo efficacy of bone-marrow-coated polycaprolactone scaffolds for the reconstruction of orbital defects in the pig. *J Biomed Mater Res B Appl Biomater* **2003**, *66*, 574-580, doi:10.1002/jbm.b.10037.
67. Williams, J.M.; Adewunmi, A.; Schek, R.M.; Flanagan, C.L.; Krebsbach, P.H.; Feinberg, S.E.; Hollister, S.J.; Das, S. Bone tissue engineering using polycaprolactone scaffolds fabricated via selective laser sintering. *Biomaterials* **2005**, *26*, 4817-4827, doi:10.1016/j.biomaterials.2004.11.057.
68. Ba Linh, N.T.; Min, Y.K.; Lee, B.T. Hybrid hydroxyapatite nanoparticles-loaded PCL/GE blend fibers for bone tissue engineering. *J Biomater Sci Polym Ed* **2013**, *24*, 520-538, doi:10.1080/09205063.2012.697696.
69. Keivani, F.; Shokrollahi, P.; Zandi, M.; Irani, S.; Shokrolahi, F.; Khorasani, S.C. Engineered electrospun poly(caprolactone)/polycaprolactone-g-hydroxyapatite nano-fibrous scaffold promotes human fibroblasts adhesion and proliferation. *Mater Sci Eng C Mater Biol Appl* **2016**, *68*, 78-88, doi:10.1016/j.msec.2016.05.098.
70. Lam, C.X.; Hutmacher, D.W.; Schantz, J.T.; Woodruff, M.A.; Teoh, S.H. Evaluation of polycaprolactone scaffold degradation for 6 months in vitro and in vivo. *J Biomed Mater Res A* **2009**, *90*, 906-919, doi:10.1002/jbm.a.32052.
71. Wutticharoenmongkol, P.; Pavasant, P.; Supaphol, P. Osteoblastic phenotype expression of MC3T3-E1 cultured on electrospun polycaprolactone fiber mats filled with hydroxyapatite nanoparticles. *Biomacromolecules* **2007**, *8*, 2602-2610, doi:10.1021/bm700451p.

72. Petretta, M.; Gambardella, A.; Boi, M.; Berni, M.; Cavallo, C.; Marchiori, G.; Maltarello, M.C.; Bellucci, D.; Fini, M.; Baldini, N.; et al. Composite Scaffolds for Bone Tissue Regeneration Based on PCL and Mg-Containing Bioactive Glasses. *Biology (Basel)* **2021**, *10*, doi:10.3390/biology10050398.
73. Hristov, V.; Radev, L.; Samuneva, B.; Apostolov, G. Organic / inorganic bioactive materials Part I: Synthesis, structure and in vitro assessment of collagen/silicocarnotite biocoatings. *Open Chemistry* **2009**, *7*, 702-710, doi:doi:10.2478/s11532-009-0067-2.
74. Rezwan, K.; Chen, Q.Z.; Blaker, J.J.; Boccaccini, A.R. Biodegradable and bioactive porous polymer/inorganic composite scaffolds for bone tissue engineering. *Biomaterials* **2006**, *27*, 3413-3431, doi:10.1016/j.biomaterials.2006.01.039.
75. Chen, Z.; Liu, Y.; Huang, J.; Wang, H.; Hao, M.; Hu, X.; Qian, X.; Fan, J.; Yang, H.; Yang, B. Enhanced In Vitro Biocompatible Polycaprolactone/Nano-Hydroxyapatite Scaffolds with Near-Field Direct-Writing Melt Electrospinning Technology. *Journal of Functional Biomaterials* **2022**, *13*, 161.
76. Sola, A.; Bertacchini, J.; D'Avella, D.; Anselmi, L.; Maraldi, T.; Marmiroli, S.; Messori, M. Development of solvent-casting particulate leaching (SCPL) polymer scaffolds as improved three-dimensional supports to mimic the bone marrow niche. *Materials Science and Engineering: C* **2019**, *96*, 153-165, doi:https://doi.org/10.1016/j.msec.2018.10.086.
77. Jiao, Z.; Luo, B.; Xiang, S.; Ma, H.; Yu, Y.; Yang, W. 3D printing of HA / PCL composite tissue engineering scaffolds. *Advanced Industrial and Engineering Polymer Research* **2019**, *2*, 196-202, doi:https://doi.org/10.1016/j.aiepr.2019.09.003.
78. Roohani-Esfahani, S.-I.; Nouri-Khorasani, S.; Lu, Z.; Appleyard, R.; Zreiqat, H. The influence hydroxyapatite nanoparticle shape and size on the properties of biphasic calcium phosphate scaffolds coated with hydroxyapatite–PCL composites. *Biomaterials* **2010**, *31*, 5498-5509.
79. Cui, Z.; Nelson, B.; Peng, Y.; Li, K.; Pilla, S.; Li, W.-J.; Turng, L.-S.; Shen, C. Fabrication and characterization of injection molded poly (ε-caprolactone) and poly (ε-caprolactone)/hydroxyapatite scaffolds for tissue engineering. *Materials Science and Engineering: C* **2012**, *32*, 1674-1681.
80. Chuenjitkuntaworn, B.; Inrung, W.; Damrongsri, D.; Mekaapiruk, K.; Supaphol, P.; Pavasant, P. Polycaprolactone/hydroxyapatite composite scaffolds: preparation, characterization, and in vitro and in vivo biological responses of human primary bone cells. *Journal of Biomedical Materials Research Part A: An Official Journal of The Society for Biomaterials, The Japanese Society for Biomaterials, and The Australian Society for Biomaterials and the Korean Society for Biomaterials* **2010**, *94*, 241-251.
81. Gerdes, S.; Mostafavi, A.; Ramesh, S.; Memic, A.; Rivero, I.V.; Rao, P.; Tamayol, A. Process–structure–quality relationships of three-dimensional printed poly (caprolactone)-hydroxyapatite scaffolds. *Tissue Engineering Part A* **2020**, *26*, 279-291.
82. Janvikul, W.; Uppanan, P.; Thavornyutikarn, B.; Kosorn, W.; Kaewkong, P. Effects of surface topography, hydrophilicity and chemistry of surface-treated PCL scaffolds on chondrocyte infiltration and ECM production. *Procedia Engineering* **2013**, *59*, 158-165.
83. Ufere, S.K.J.; Sultana, N. Contact angle, conductivity and mechanical properties of polycaprolactone/hydroxyapatite/polypyrrole scaffolds using freeze-drying technique. *ARPN J. Eng. Appl. Sci* **2016**, *11*, 13686.
84. Jiang, W.; Shi, J.; Li, W.; Sun, K. Morphology, wettability, and mechanical properties of polycaprolactone/hydroxyapatite composite scaffolds with interconnected pore structures fabricated by a mini-deposition system. *Polymer Engineering & Science* **2012**, *52*, 2396-2402.
85. Eosoly, S.; Lohfeld, S.; Brabazon, D. Effect of hydroxyapatite on biodegradable scaffolds fabricated by SLS. In Proceedings of the Key Engineering Materials, 2009; pp. 659-662.
86. Renghini, C.; Komlev, V.; Fiori, F.; Verné, E.; Baino, F.; Vitale-Brovarone, C. Micro-CT studies on 3-D bioactive glass–ceramic scaffolds for bone regeneration. *Acta Biomaterialia* **2009**, *5*, 1328-1337, doi:https://doi.org/10.1016/j.actbio.2008.10.017.
87. Abbasi, N.; Hamlet, S.; Love, R.M.; Nguyen, N.-T. Porous scaffolds for bone regeneration. *Journal of Science: Advanced Materials and Devices* **2020**, *5*, 1-9, doi:https://doi.org/10.1016/j.jsamd.2020.01.007.
88. Cheng, M.-q.; Wahafu, T.; Jiang, G.-f.; Liu, W.; Qiao, Y.-q.; Peng, X.-c.; Cheng, T.; Zhang, X.-l.; He, G.; Liu, X.-y. A novel open-porous magnesium scaffold with controllable microstructures and properties for bone regeneration. *Scientific reports* **2016**, *6*, 1-14.
89. Iviglia, G.; Kargozar, S.; Baino, F. Biomaterials, current strategies, and novel nano-technological approaches for periodontal regeneration. *Journal of functional biomaterials* **2019**, *10*, 3.
90. Aliotta, L.; Cinelli, P.; Coltelli, M.B.; Righetti, M.C.; Gazzano, M.; Lazzeri, A. Effect of nucleating agents on crystallinity and properties of poly (lactic acid) (PLA). *European Polymer Journal* **2017**, *93*, 822-832, doi:https://doi.org/10.1016/j.eurpolymj.2017.04.041.
91. Dziadek, M.; Menaszek, E.; Zagrajczuk, B.; Pawlik, J.; Cholewa-Kowalska, K. New generation poly(ε-caprolactone)/gel-derived bioactive glass composites for bone tissue engineering: Part I. Material properties. *Mater Sci Eng C Mater Biol Appl* **2015**, *56*, 9-21, doi:10.1016/j.msec.2015.06.020.
92. Abifarin, J.K.; Obada, D.O.; Dauda, E.T.; Dodoo-Arhin, D. Experimental data on the characterization of hydroxyapatite synthesized from biowastes. *Data in Brief* **2019**, *26*, 104485, doi:https://doi.org/10.1016/j.dib.2019.104485.
93. Eric, M.R.-M.o. Hydroxyapatite-Based Materials: Synthesis and Characterization. In *Biomedical Engineering*, Reza, F.-R., Ed.; IntechOpen: Rijeka, 2011; p. Ch. 4.
94. Du, J.; Zuo, Y.; Lin, L.; Huang, D.; Niu, L.; Wei, Y.; Wang, K.; Lin, Q.; Zou, Q.; Li, Y. Effect of hydroxyapatite fillers on the mechanical properties and osteogenesis capacity of bio-based polyurethane composite scaffolds. *Journal of the Mechanical Behavior of Biomedical Materials* **2018**, *88*, 150-159, doi:https://doi.org/10.1016/j.jmbbm.2018.08.028.

95. Osuchukwu, O.A.; Salihi, A.; Abdullahi, I.; Abdulkareem, B.; Nwannenna, C.S. Synthesis techniques, characterization and mechanical properties of natural derived hydroxyapatite scaffolds for bone implants: a review. *SN Applied Sciences* **2021**, *3*, 822, doi:10.1007/s42452-021-04795-y.
96. Kim, J.; Magno, M.H.; Waters, H.; Doll, B.A.; McBride, S.; Alvarez, P.; Darr, A.; Vasanji, A.; Kohn, J.; Hollinger, J.O. Bone regeneration in a rabbit critical-sized calvarial model using tyrosine-derived polycarbonate scaffolds. *Tissue Eng Part A* **2012**, *18*, 1132-1139, doi:10.1089/ten.TEA.2011.0582.
97. Nicoll, S. Materials for Bone Graft Substitutes and Osseous Tissue Regeneration. 2011; pp. 343-362.
98. Caseiro, A.; Alvites, R.; Pedrosa, S.; Miguel, J.; Reis, I.; Santos, J.; Mendonça, C.; Atayde, M.; Maurício, A. The potential clinical application of mesenchymal stem cells from the dental pulp (DPSCs) for bone regeneration. *Frontiers in Stem Cell and Regenerative Medicine Research* **2017**, *6*, 3-52.
99. Caseiro, A.R.; Santos Pedrosa, S.; Ivanova, G.; Vieira Branquinho, M.; Almeida, A.; Faria, F.; Amorim, I.; Pereira, T.; Maurício, A.C. Mesenchymal Stem/ Stromal Cells metabolomic and bioactive factors profiles: A comparative analysis on the umbilical cord and dental pulp derived Stem/ Stromal Cells secretome. *PLoS One* **2019**, *14*, e0221378, doi:10.1371/journal.pone.0221378.
100. Yang, X.; Yang, F.; Walboomers, X.F.; Bian, Z.; Fan, M.; Jansen, J.A. The performance of dental pulp stem cells on nanofibrous PCL/gelatin/nHA scaffolds. *J Biomed Mater Res A* **2010**, *93*, 247-257, doi:10.1002/jbm.a.32535.
101. Aghazadeh, M.; Samiei, M.; Hokmabad, V.R.; Alizadeh, E.; Jabbari, N.; Seifalian, A.; Salehi, R. The Effect of Melanocyte Stimulating Hormone and Hydroxyapatite on Osteogenesis in Pulp Stem Cells of Human Teeth Transferred into Polyester Scaffolds. *Fibers and Polymers* **2018**, *19*, 2245-2253, doi:10.1007/s12221-018-8309-6.
102. Park, S.; Kim, J.E.; Han, J.; Jeong, S.; Lim, J.W.; Lee, M.C.; Son, H.; Kim, H.B.; Choung, Y.-H.; Seonwoo, H.; et al. 3D-Printed Poly(ε-Caprolactone)/Hydroxyapatite Scaffolds Modified with Alkaline Hydrolysis Enhance Osteogenesis In Vitro. *Polymers* **2021**, *13*, 257.
103. Rosales-Ibáñez, R.; Cubo-Mateo, N.; Rodríguez-Navarrete, A.; González-González, A.M.; Villamar-Duque, T.E.; Flores-Sánchez, L.O.; Rodríguez-Lorenzo, L.M. Assessment of a PCL-3D Printing-Dental Pulp Stem Cells Triplet for Bone Engineering: An In Vitro Study. *Polymers* **2021**, *13*, 1154.
104. Jensen, J.; Kraft, D.C.; Lysdahl, H.; Foldager, C.B.; Chen, M.; Kristiansen, A.A.; Rölfing, J.H.; Bünger, C.E. Functionalization of polycaprolactone scaffolds with hyaluronic acid and β-TCP facilitates migration and osteogenic differentiation of human dental pulp stem cells in vitro. *Tissue Eng Part A* **2015**, *21*, 729-739, doi:10.1089/ten.TEA.2014.0177.
105. Soriente, A.; Amodio, S.P.; Fasolino, I.; Raucci, M.G.; Demitri, C.; Engel, E.; Ambrosio, L. Chitosan/PEGDA based scaffolds as bioinspired materials to control in vitro angiogenesis. *Materials Science and Engineering: C* **2021**, *118*, 111420, doi:https://doi.org/10.1016/j.msec.2020.111420.
106. Tang, A.; Li, J.; Li, J.; Zhao, S.; Liu, W.; Liu, T.; Wang, J.; Liu, Y. Nanocellulose/PEGDA aerogel scaffolds with tunable modulus prepared by stereolithography for three-dimensional cell culture. *Journal of Biomaterials Science, Polymer Edition* **2019**, *30*, 797-814, doi:10.1080/09205063.2019.1602904.
107. Zhang, X.; Yan, Z.; Guan, G.; Lu, Z.; Yan, S.; Du, A.; Wang, L.; Li, Q. Polyethylene glycol diacrylate scaffold filled with cell-laden methacrylamide gelatin/alginate hydrogels used for cartilage repair. *Journal of Biomaterials Applications* **2022**, *36*, 1019-1032, doi:10.1177/08853282211044853.